ELSEVIER

Journal of Biomechanics 36 (2003) 103–112

JOURNAL OF BIOMECHANICS

www.elsevier.com/locate/jbiomech
www.JBiomech.com

A three-dimensional computational analysis of fluid–structure interaction in the aortic valve

J. De Hart*, G.W.M. Peters, P.J.G. Schreurs, F.P.T. Baaijens

Department of Biomedical Engineering, Eindhoven University of Technology, Building W-hoog-4.117, P.O. Box 513, 5600 MB Eindhoven, The Netherlands

Accepted 27 June 2002

Abstract

Numerical analysis of the aortic valve has mainly been focused on the closing behaviour during the diastolic phase rather than the kinematic opening and closing behaviour during the systolic phase of the cardiac cycle. Moreover, the fluid–structure interaction in the aortic valve system is most frequently ignored in numerical modelling. The effect of this interaction on the valve's behaviour during systolic functioning is investigated. The large differences in material properties of fluid and structure and the finite motion of the leaflets complicate blood–valve interaction modelling. This has impeded numerical analyses of valves operating under physiological conditions. A numerical method, known as the Lagrange multiplier based fictitious domain method, is used to describe the large leaflet motion within the computational fluid domain. This method is applied to a three-dimensional finite element model of a stented aortic valve. The model provides both the mechanical behaviour of the valve and the blood flow through it. Results show that during systole the leaflets of the stented valve appear to be moving with the fluid in an essentially kinematical process governed by the fluid motion.

Keywords: Aortic valve; Fluid–structure interaction; Finite element method; Fictitious domain method; Three-dimensional analysis

1. Introduction

Many numerical structural models have been developed that describe the behaviour of the aortic valve ignoring its interaction with the blood, e.g. see Black et al. (1991); Chandran et al. (1991); Krucinski et al. (1993); De Hart et al. (1998); Cacciola et al. (2000). The valve opening and closing during systole involves, however, a strong interaction between blood and the surrounding tissue. Several attempts have been made to analyse the valve behaviour using numerical fluid–structure interaction models, e.g. see Horsten (1990); Peskin and McQueen (1995); Makhijani et al. (1997). A detailed three-dimensional analysis of the valve kinematics, mechanics and fluid dynamics during the systolic phase has not been reported to date.

Modelling of such a fluid–structure interaction system is complicated due to the large motion of the thin leaflets through the computational fluid domain. The mathematical formulation of the equation of motion for a fluid is most conveniently described with respect to an Eulerian reference frame. However, this is incompatible with the Lagrangian formulation which is more appropriate to describe a structural phase. The arbitrary Lagrangian–Eulerian (ALE) method, first proposed by Donea et al. (1982), effectively combines the two different formulations and is frequently used in fluid–structure interaction analyses. Applied to the fluid phase, the ALE method requires a continuous adaptation of the fluid mesh without modification of the topology. Due to the large leaflet motions it is, however, difficult to adapt the fluid mesh in such a way that a proper mesh quality is maintained without changing the topology. Alternatively, remeshing of the fluid domain may be performed in conjunction with an ALE method, where remeshing is only performed if the mesh has degenerated too much. The change in topology during remeshing requires the use of interpolation techniques to recover state variables on the newly generated mesh. This not only introduces artificial diffusivity, but is also

*Corresponding author. Tel.: +31-40-2473135; fax: +31-40-2447355.
E-mail address: j.d.hart@tue.nl (J. De Hart).

0021-9290/02/$ - see front matter
PII: S0021-9290(02)00244-0

difficult and/or time-consuming to perform with sufficient robustness and accuracy for three-dimensional problems.

To resolve the limitations of these mesh update strategies we use a fictitious domain method to describe the interaction of the leaflets with the fluid. In this method, the different mathematical descriptions for the fluid and structure can be maintained, allowing convenient classical formulations for each of these subsystems. Moreover, the fluid mesh is not altered or interrupted by the presence of the immersed domain, and therefore preserves its original quality. Experimental validation of this method applied to a two-dimensional aortic valve model is demonstrated by De Hart et al. (2000). The application to a three-dimensional isotropic valve with rigid aortic root (mimicking a stented valve) and trileaflet symmetry is described in this paper. The model is used to study the effect of fluid–structure interaction on the valve behaviour for a reduced Reynolds number flow. We intend to address the importance of systolic functioning on the valve's (life-long) functionality. To this end, the influence of the fluid-structure interaction on the valve kinematics is investigated and the impact on the structural stress state and the associated fluid dynamical flow is analysed.

2. Methods

The blood flow is considered to be isothermal and incompressible. Assuming a Newtonian constitutive behaviour (Caro et al., 1978), the flow within the domain Ω_f bounded by Γ_f can be described by the well-known Navier–Stokes equation and continuity equation:

$$\begin{aligned} &\rho_f\left(\frac{\partial \vec{v}_f}{\partial t}+\vec{v}_f\cdot\vec{\nabla}\vec{v}_f\right)=-\vec{\nabla}p_f+\vec{\nabla}\cdot 2\eta_f\boldsymbol{D}_f \quad \text{in } \Omega_f,\\ &\vec{\nabla}\cdot\vec{v}_f=0 \qquad\qquad\qquad\qquad\qquad\qquad\quad \text{in } \Omega_f, \end{aligned} \tag{1}$$

where ρ_f denotes the density, t the time, $\vec{v}_f$ is the velocity, $\vec{\nabla}$ the gradient operator with respect to the current configuration, p_f the pressure, η_f the dynamic viscosity of the fluid and $\boldsymbol{D}_f$ the rate-of-deformation tensor defined as $\boldsymbol{D}_f=1/2(\vec{\nabla}\vec{v}_f+(\vec{\nabla}\vec{v}_f)^T)$. In this formulation body forces are neglected. Clearly, the above set of equations must be supplemented with appropriate boundary conditions (see next section).

The aortic valve leaflets are assumed to behave linear elastic and isotropic according to a Neo-Hookean constitutive model. Hence, in absence of body forces and with inertia terms neglected, the equation of motion and the continuity equation for the incompressible structural domain Ω_s bounded by Γ_s read

$$\begin{aligned} &\vec{\nabla}\cdot(-p_s\boldsymbol{I}+G(\boldsymbol{B}-\boldsymbol{I}))=\vec{0} \quad \text{in } \Omega_s,\\ &\det(\boldsymbol{F})=1 \qquad\qquad\qquad\qquad\quad \text{in } \Omega_s, \end{aligned} \tag{2}$$

where p_s denotes the hydrostatic pressure, $\boldsymbol{I}$ the second-order unit tensor, G the shear modulus and $\boldsymbol{B}$ the Finger or left Cauchy–Green strain tensor. The deformation tensor is defined as $\boldsymbol{F}=(\vec{\nabla}_0\vec{x})^T$, with $\vec{\nabla}_0$ the gradient operator with respect to the initial configuration and $\vec{x}$ the field of material points. Also this set of equations must be completed with suitable boundary conditions.

For the structural domain an updated Lagrange formulation is used to describe the deformation throughout the time span of the analysis (Baaijens, 2001). In this formulation it is customary to take the displacement field $\vec{u}$ as the unknown. During a time interval $t^n \to t^{n+1}$ this field is defined as

$$\vec{u}=\vec{x}^{n+1}-\vec{x}^{n}, \tag{3}$$

where $\vec{x}^n$ and $\vec{x}^{n+1}$ denote the position of a material point at time $t=t^n$ and $t=t^{n+1}$, respectively. In view of the fluid–structure interaction the structural velocity field is considered rather than the displacement field. Hence, the velocity during time step $\Delta t=t^{n+1}-t^n$ is defined as

$$\vec{v}_s=\frac{1}{\Delta t}(\vec{x}^{n+1}-\vec{x}^{n})=\frac{\vec{u}}{\Delta t}, \tag{4}$$

which represents a first-order approximation for the structural velocity field.

Consider the domain Ω_s^i, with fluid–structure interface boundary γ^i, to be the part of Ω_s immersed in Ω_f, see Fig. 1. Then fluid–structure coupling is realized by enforcing the (no-slip) constraint

$$\vec{v}_f-\vec{v}_s=\vec{0} \text{ on } \gamma^i. \tag{5}$$

Physically Ω_f and Ω_s^i cannot occupy the same domain in space; interaction occurs only at the interface γ^i. Thus, a new definition for the fluid domain would hold: $\Omega_f^*=\Omega_f\backslash\Omega_s^i$. In fluid–structure interaction analysis the sets of (1), (2) and the no-slip constraint (5) are most commonly employed with the fluid domain defined as $\Omega_f\backslash\Omega_s^i$. using for example an ALE technique. The basic idea of the fictitious domain method is to extend the fluid problem defined in $\Omega_f\backslash\Omega_s^i$ to a problem defined in all of Ω_f, while still forcing the solution to satisfy (5). However, the fluid contents enclosed by Ω_s^i may not

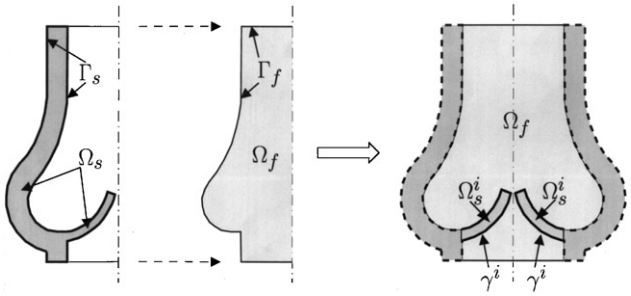

Fig. 1. Sample of an immersed domain Ω_s^i with boundary γ^i in Ω_f.

affect the structural deformation, since it is physically not present. On the other hand, the enclosed fluid contents must move according to the inner structural deformation, to preserve conservation of fluid mass. For thin-walled structures, such as the leaflets, the complications arising from enclosing a part of the fluid domain may be neglected, since the inner fluid volume is much smaller than the outside volume. Moreover, assuming the thickness to be negligible as far as the interaction with the fluid is considered, alignment of the interface γ^{i} with one side of the leaflet is particularly suitable. Hence, in a fictitious domain formulation of the aortic valve leaflets the definition Ω_{f} for the entire fluid domain, including the immersed structures, can be maintained.

The constraint Eq. (5) must be incorporated into the formulations of the fluid and structural problem. Here the Lagrange multiplier $\vec{\lambda}$ is used to weakly enforce the coupling constraint on the fluid–structure interface γ^{i}. Within the framework of the finite element method (FEM) the weak form of the resulting set of equations is then given by

$$\begin{aligned}
&\int_{\Omega_{\mathrm{f}}} \vec{w}_f \cdot \left(\rho_{\mathrm{f}} \frac{\partial \vec{v}_{\mathrm{f}}}{\partial t} + \rho_{\mathrm{f}} \vec{v}_{\mathrm{f}} \cdot \vec{\nabla} \vec{v}_{\mathrm{f}} \right) \mathrm{d}\Omega_{\mathrm{f}} \\
&\quad + \int_{\Omega_{\mathrm{f}}} (\vec{\nabla} \vec{w}_{\mathrm{f}})^{\mathrm{T}} : 2\eta \boldsymbol{D}_{\mathrm{f}} \, \mathrm{d}\Omega_{\mathrm{f}} - \int_{\Omega_{\mathrm{f}}} p_{\mathrm{f}} \cdot \vec{\nabla} \cdot \vec{w}_{\mathrm{f}} \, \mathrm{d}\Omega_{\mathrm{f}} \\
&\quad + \int_{\Gamma_{\mathrm{f}}} \vec{w}_{\mathrm{f}} \cdot \vec{t}_{\mathrm{f}} \, \mathrm{d}\Gamma_{\mathrm{f}} + \int_{\gamma^{\mathrm{i}}} \vec{\lambda} \cdot \vec{w}_{\mathrm{f}} \, \mathrm{d}\gamma^{\mathrm{i}} = 0, \\
&\int_{\Omega_{\mathrm{f}}} q_{\mathrm{f}} . \vec{\nabla} \cdot \vec{v}_{\mathrm{f}} \, \mathrm{d}\Omega_{\mathrm{f}} = 0,
\end{aligned} \tag{6}$$

$$\begin{aligned}
&\int_{\Omega_{\mathrm{s}}} (\vec{\nabla} \vec{w}_{\mathrm{s}})^{\mathrm{T}} : (G(\boldsymbol{B} - \boldsymbol{I})) \, \mathrm{d}\Omega_{\mathrm{s}} \\
&\quad - \int_{\Omega_{\mathrm{s}}} p_{\mathrm{s}} \cdot \vec{\nabla} \cdot \vec{w}_{\mathrm{s}} \, \mathrm{d}\Omega_{\mathrm{s}} - \int_{\gamma^{\mathrm{i}}} \vec{\lambda} \cdot \vec{w}_{\mathrm{s}} \, \mathrm{d}\gamma^{\mathrm{i}} = 0, \\
&\int_{\Omega_{\mathrm{s}}} q_{\mathrm{s}} \cdot (\det(\boldsymbol{F}) - 1) \, \mathrm{d}\Omega_{\mathrm{s}} = 0,
\end{aligned} \tag{7}$$

$$\int_{\gamma^{\mathrm{i}}} \vec{\ell} \cdot (\vec{v}_{\mathrm{f}} - \vec{v}_{\mathrm{s}}) \, \mathrm{d}\gamma^{\mathrm{i}} = 0, \tag{8}$$

which must hold for all admissible weighting functions $\vec{w}_{\mathrm{f}}$, q_{f}, $\vec{w}_{\mathrm{s}}$, q_{s} and $\vec{\ell}$. In this formulation $\vec{\lambda}$ may be interpreted as the surface force exerted on the fluid and structure along γ^{i} to maintain the coupling between them and $\vec{t}_{\mathrm{f}}$ represents the surface tractions operating on the fluid boundary Γ_{f}.

The spatial discretizations of the fluid domain (denoted by $\mathscr{T}_{\mathrm{f}}$) and structural domain (denoted by $\mathscr{T}_{\mathrm{s}}$) are based on hexahedral elements with a triquadratic approximation of the velocity and displacement field and a linear, but discontinuous approximation of the pressures (Crouzeix–Raviart family). The discretization of the thin-walled valve leaflets requires that the element aspect ratio, defined as the ratio between the smallest and largest dimension of an element, should not exceed 1:7 to obtain a correct bending behaviour. Numerical experiments showed that larger ratios introduce artificial stiffness leading to an incorrect motion of the leaflets.

The discretizations $\mathscr{T}_{\mathrm{f}}$ and $\mathscr{T}_{\mathrm{s}}$ can be chosen irrespective of each other. Moreover, the discretization of the Lagrange multipliers, i.e. $\mathscr{T}_{\gamma^{\mathrm{i}}}$, that operate on the fluid–structure boundary γ^{i} can be chosen independent of $\mathscr{T}_{\mathrm{f}}$ and $\mathscr{T}_{\mathrm{s}}$. This kind of decoupling between $\mathscr{T}_{\mathrm{f}}$, $\mathscr{T}_{\mathrm{s}}$ and $\mathscr{T}_{\gamma^{\mathrm{i}}}$ makes the fictitious domain approach very attractive for problems with moving boundaries. However, $\mathscr{T}_{\gamma^{\mathrm{i}}}$ has to be chosen such that it does not introduce spurious modes or locking in the other degrees of freedom of the velocity field (Brezzi, 1974), and is therefore subjected to similar stability considerations as the discretization of the pressure degrees of freedom in the mixed formulation. So, here we encounter the limitation of the fictitious domain method. Stability reasons require for the mesh sizes that $h_{\Omega_{\mathrm{f}}} < h_{\gamma^{\mathrm{i}}}$ and $h_{\Omega_{\mathrm{s}}} < h_{\gamma^{\mathrm{i}}}$. However, accuracy with respect to fluid–structure coupling is enhanced by requiring $h_{\Omega_{\mathrm{f}}} > h_{\gamma^{\mathrm{i}}}$ and $h_{\Omega_{\mathrm{s}}} > h_{\gamma^{\mathrm{i}}}$. As a result it is complicated to generate a discretization of the (moving) surface on which the Lagrange multiplier is applied.

In De Hart et al. (2000), where $h_{\Omega_{\mathrm{f}}} \approx h_{\Omega_{\mathrm{s}}}$ was used, this discrepancy is dealt with by choosing the discretization of $\vec{\lambda}$, and hence also $\vec{\ell}$, linear, discontinuous and spatially coincident with element boundaries of the structural domain. In general, the interpolation of the Lagrange multiplier field should be chosen at least one order lower than the interpolation order of the velocity and displacement field, as otherwise locking in the other degrees of freedom is introduced.

Considering the restrictions of the aspect ratio for $\mathscr{T}_{\mathrm{s}}$, the relation between the mesh sizes $h_{\Omega_{\mathrm{f}}}$ and $h_{\Omega_{\mathrm{s}}}$ is such that $h_{\Omega_{\mathrm{f}}} > h_{\Omega_{\mathrm{s}}}$. Consequently, a discretization as used by De Hart et al. (2000) is not applied here. Instead, each component of $\vec{\lambda}$ is approximated with a piecewise constant, making the distance between two points in $\mathscr{T}_{\gamma^{\mathrm{i}}}$ less constrained. Here, N control points $\vec{x}_{\lambda_k}$, $k = 1, 2, \ldots, N$ are introduced on the boundary γ^{i} and positioned in the centres of the structural element sides coinciding with γ^{i} (Fig. 2). At these control points the fluid–structure coupling (5) is enforced. For each point at which the Lagrange multiplier related constant is computed, the structural velocity is obtained trivially since the spatial location of the control point coincides with the centre of the associated structural element side along γ^{i} (Fig. 2). However, the interpolation of the fluid velocity to the control points must be computed. This requires identification of the fluid element and the isoparametric coordinates of the fluid particle coincident with the spatial location of the control point. Once these coordinates are known, the fluid velocity at the control

point can be expressed in terms of the nodal fluid velocities.

Time discretization of (6) is achieved using an implicit, backward-Euler scheme. Consider the time interval $t^n \to t^{n+1}$, with time step $\Delta t = t^{n+1} - t^n$, then

$$\frac{\partial \vec{v}_f}{\partial t} \approx \frac{\vec{v}_f^{n+1} - \vec{v}_f^n}{\Delta t}. \tag{9}$$

This choice leads to a scheme that is first-order accurate in time.

The problem defined by (6) to (8) renders a non-linear system of algebraic equations which is linearized using Newton's method. The procedure used in this work to solve this coupled problem is based on a fully coupled approach using a BiCGStab iterative solver with a preconditioner according to an incomplete LU factorization (Saad, 1996). Hence, the fluid unknowns, structural unknowns and Lagrange multipliers are solved simultaneously based on the integrated method (Cuvelier et al., 1986). Within each time step a Newton–Raphson iterative procedure is adopted to obtain a converged solution with respect to the fluid and structural velocity fields, the pressure fields and Lagrange multipliers. At each iteration the velocity field of the structure is fully coupled to the velocity field of the fluid. As a result, numerical instabilities, which will be discussed briefly hereafter, are circumvented. During the iterative procedure the fluid–structure coupling through Eq. (8) is enforced using the location of γ^i defined at the beginning of the current time step. Enforcement on the most recently computed location of γ^i, as employed in the two-dimensional case (De Hart et al., 2000), reduces the convergence rate in the three-dimensional application leading to a computationally inefficient procedure.

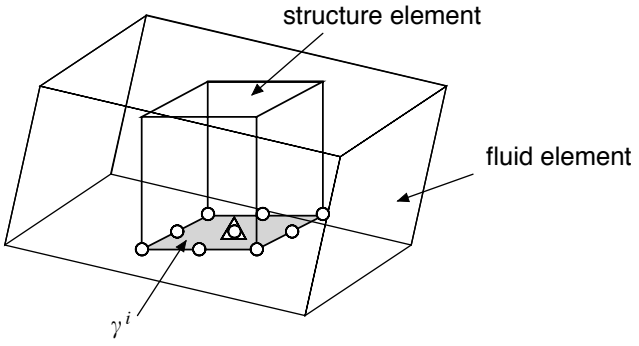

Fig. 2. Sample of a structural element inside a fluid element. The structural nodal points at the interface γ^i are denoted by ○. The control point at which the Lagrange multiplier is defined is denoted by △.

A weakly coupled strategy to solve the fluid and structural problem separately, as used in the staggered procedures described by Felippa et al. (1998) and Lesoinne M. and Farhat (1998), fails for stability reasons. This strategy involves transport of surface tractions from the fluid domain to the structural domain and displacement fields vice versa (Farhat et al., 1998; Rutten, 1998; Wall and Ekkehard, 1998). During the opening and closing phase of the aortic valve the leaflets show very low resistance to bending. Enforcing the surface tractions computed from the fluid problem will result in an overestimated displacement field for the leaflet to obtain internal stresses that balance the tractions. Application of this displacement field to the fluid domain invokes instability of the system. An alternative strategy involves transport of the computed fluid velocity field to the structural domain. However, the leaflet structure is designed to bear tensile stresses rather than compressive stresses. Consequently, application of the computed fluid velocity field to the leaflet structure may introduce unrealistic internal stresses, which would lead to erroneous results initiating instability when coupled back to the fluid. Attempts to make these, from a computational point of view, efficient procedures successful, using for example under-relaxation schemes, unfortunately failed.

For a detailed discussion on the numerical techniques adopted in this work the reader is referred to De Hart (2002).

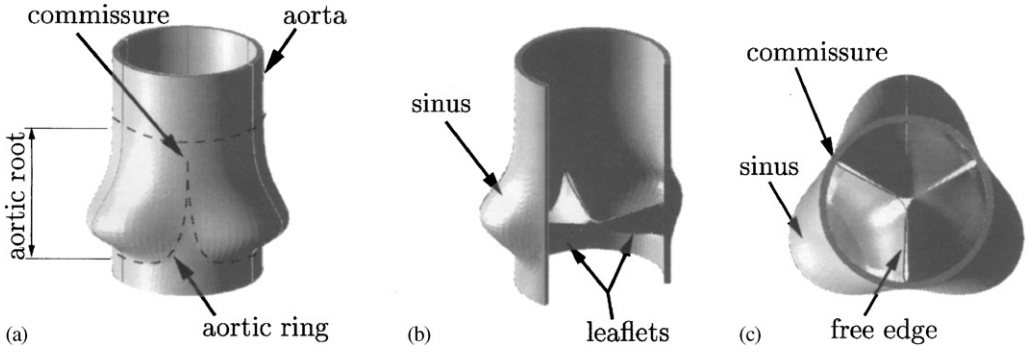

Fig. 3. Sketches of stented the aortic valve: side view of the complete valve (a), after dissection of one leaflet with corresponding sinus wall (b), and top view.

3. Model properties

The aortic valve consists of three highly flexible leaflets, which are attached to the aortic root from one commissural point along a doubly curved line (aortic ring) towards a second commissural point, as illustrated in Fig. 3(a)–(c). Behind each leaflet the aortic root bulbs into a sinus cavity to form the beginning of the ascending aorta. Fig. 4 shows the relevant dimensions, which have frequently been used to describe the geometry of the valve. The values of these dimensions, based on the geometry of prototype valves (Cacciola, 1998; De Hart et al., 1998), are summarized in Table 1. The values of the material parameters used in the model are also given in Table 1.

Although in reality the three leaflets are not precisely identical, it is assumed that they are similar enough to permit a general description of a valve with trileaflet symmetry. Hence, only $\frac{1}{6}$ of the valve is considered in the model (Fig. 5(b)), which contains approximately 20,000 fluid and 6500 structural degrees of freedom. The configuration shown in this figure is taken as the initial, stress-free condition of the model. The model is bounded in circumferential direction by the symmetry surface, which intersects through half of one leaflet, and by the contact surface, at which two adjacent leaflets come into contact during the closing phase (Fig. 5(a)). In the axial direction the model is bounded by the ventricular (inflow) and aortic (outflow) plane (Fig. 5(c)), and obviously, in radial direction by the aortic wall, which is assumed to be rigid to mimic a stented valve. The leaflet is fixed to the aortic wall using homogeneous Dirichlet conditions imposed over the full thickness of the valve. Moreover, homogeneous Dirichlet conditions are imposed to suppress out of plane motion for the fluid and leaflet at the symmetry surface and for the fluid only at the contact surface. No-slip conditions are enforced at the fluid–wall surface. The fluid–structure coupling at the contact surface prevents the leaflet from penetrating this surface for sufficiently small time steps. The application of hexahedral elements to model the leaflet has consequences for the bending behaviour at the fixation and symmetry surface. Homogeneous Dirichlet conditions are applied over the full leaflet thickness at these surfaces to simulate suppression of leaflet rotation. This approach is slightly different from using shell elements for which rotation is an explicitly defined degree of freedom. For stability reasons an extra fluid conduit is used to lengthen the in- and outflow tract. The model is loaded during the systolic phase by ventricular and aortic pressures (Fig. 6), to demonstrate the applicability of the presented method. The pressures are applied to the fluid domain at the inflow and outflow surfaces in 100 successive time steps for this time span.

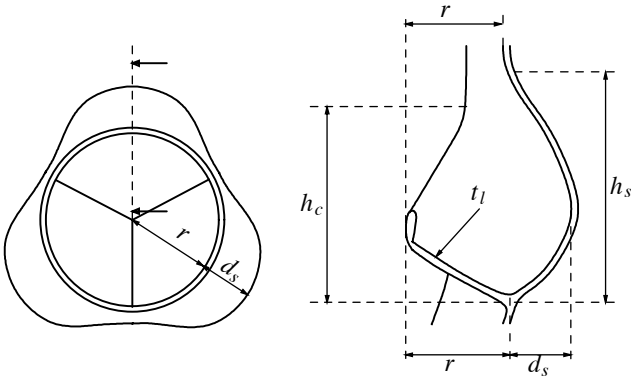

Fig. 4. Definition of relevant dimensions used to describe the geometry of the model: r denotes the valve radius, d_s the sinus depth, h_s the sinus height, h_c the commissural height and t_l the leaflet thickness.

4. Results

The valve kinematics is controlled by the surrounding fluid flow and the interaction of this flow with the leaflets, resulting in substantially different opening and closing configurations (Fig. 7). The opening behaviour is typical for stented valves (Cacciola, 1998) showing high curvatures of the free edge (Fig. 7(b)). The Reynolds number, defined as $Re = \rho_f V_r/\eta_f$, reaches a value of 900 at peak systolic mainstream velocity, i.e. $V = 300\,(\mathrm{mm/s})$ at $t = 0.065\,(\mathrm{s})$. However, the moment of complete opening corresponds to Fig. 7(c), i.e. at $t = 0.0875\,(\mathrm{s})$, showing approximately a circular orifice. The Strouhal number, defined as $Sr = r/V_\tau$, with τ (≈ 0.12) the time span from maximum systolic flow to the onset of flow reversal (Fig. 7(f)), is approximately 0.3. The physiological values of these numbers, however, read $Re \approx 4500$ and $Sr \approx 0.06$. The application of these values is not feasible in view of the rather coarse fluid mesh, which is

Table 1
Geometrical and material properties of the valve model: r denotes the valve radius, d_s the sinus depth, h_s the sinus height, h_c the commissural height, t_l the leaflet thickness, η_f the dynamic fluid viscosity, ρ_f the fluid density and G the structural shear modulus

Geometric properties					Material properties		
r (mm)	d_s (mm)	h_s (mm)	h_c (mm)	t_l (μm)	η_f (Pa s)	ρ_f (kg/m^3)	G (MPa)
12.0	5.75	21.0	10.5	200.0	4.0×10^{-3}	1.0×10^{3}	3.0×10^{-2}

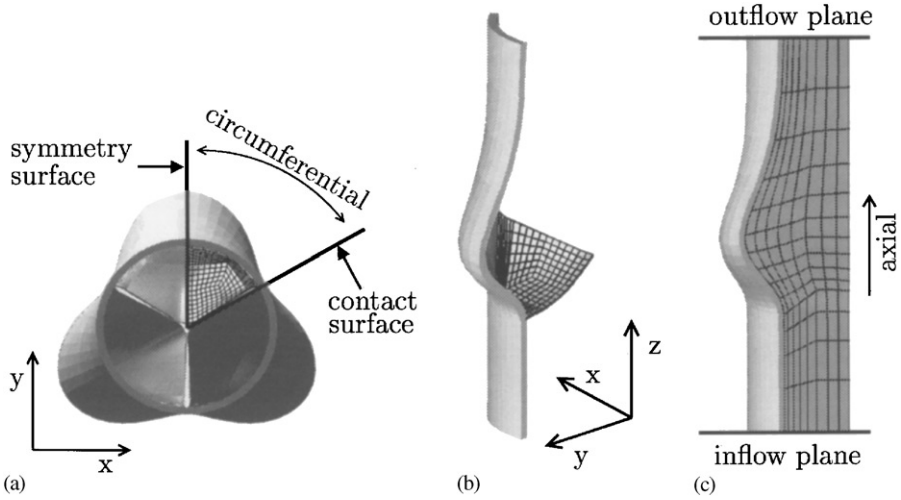

Fig. 5. Three-dimensional FEM model of the aortic heart valve: (a) part of the valve used for computation, (b) FEM mesh of the structure and (c) FEM mesh of the fluid.

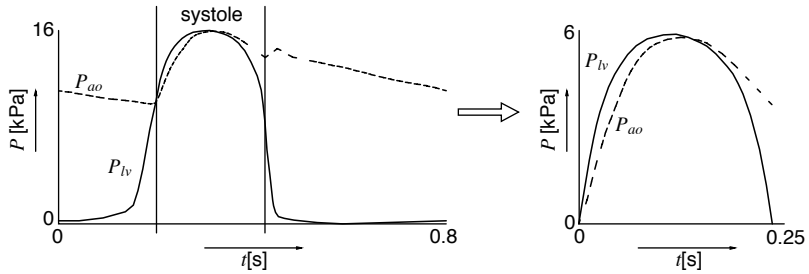

Fig. 6. Aortic (P_{ao}: dashed line) and left ventricular (P_{lv}: solid line) pressure curves during the cardiac cycle. The applied systolic pressures are given on the right hand side.

chosen such that both memory and CPU time are reasonable to demonstrate the proposed numerical method.

The kinematical differences during opening and closing result in a cyclic stress pattern of the leaflets, which is believed to be important in the analysis of fatigue behaviour (Fig. 8). During the opening of the valve (Fig. 8(a) and (b)) tensile stresses in the middle of the leaflets are more dominant on the aortic side of the leaflets, whereas compressive stresses are present at the ventricular side. This can clearly be observed (see the left-hand side figures) and is caused by the high curvature in the symmetry plane, which intersects through half of the leaflets. Similar configurations have been measured by Gao et al. (2000) monitoring the leaflet motion in bioprosthetic valves with dual camera stereo photogrammetry. Near the fixation edge, on the other hand, compressive stresses appear on the ventricular side and tensile stresses on the aortic side. The stress distribution is rather inhomogeneous during this phase. The middle frame represents the initial phase of valve closing, which shows significant stresses in the middle of the leaflet. For this configuration the compressive stresses appear on the ventricular side, whereas tensile stresses are more dominant on the aortic side. The last two frames are taken at the end of the systolic phase, where a rapid closure of the valve occurs. The stresses in the leaflets are significantly increasing in this phase as they have to bear the increasing pressure gradient across the valve. As stated before, the simulation does not include the diastolic phase. Moreover, with the applied material parameters, the leaflet would undergo excessive deformations to balance the diastolic pressure gradient. In reality, the natural valve shows a complex fibre-reinforced composite texture to be able to bear diastolic pressures.

The interaction of the valve with the fluid and the application of the time-dependent pressure curves result in a complex three-dimensional flow, which shows vortical flow development near the leaflet free edge and in the sinus cavity (Fig. 9). The initial (stress-free) configuration (frame (a)) corresponds to a closed valve. During the acceleration phase (frame (b)) a forward flow is observed for every point of the fluid domain, including in the sinus cavity (i.e. wash-out). For the fully opened valve (frame (c)) the flow is more central

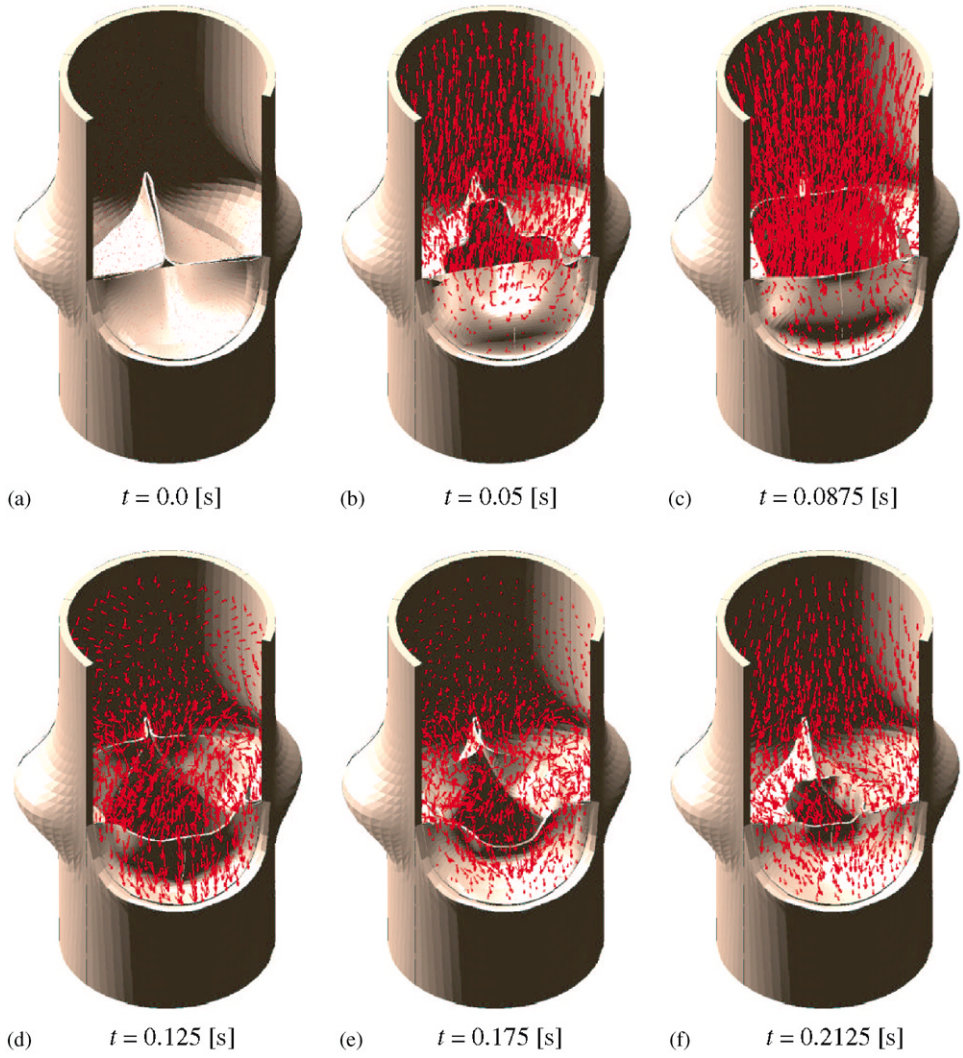

Fig. 7. Configurations of the stented valve taken at six successive time points during the systolic phase. The fluid velocity vector field is also shown.

and very little flow in the sinus cavity is observed. At the moment of complete valve opening, however, the flow has started to decelerate already. During the deceleration phase recirculation at the leaflet free edge precedes vortex development in the sinus cavity and the valve is driven to a closed position (frames (d) and (e)). Similar results were found by Van Steenhoven and Veenstra (1982) for in vivo experiments with approximately the same peak systolic velocity. A completely closed valve is obtained after reversal of the pressure gradient, leading to a little amount of back flow (frame (f)). This last phase of the leaflets motion results in a quick final closure of the valve.

5. Discussion

A three-dimensional fictitious domain method is applied to model fluid–structure interaction in the aortic valve. The method is based on the imposition of kinematical constraints, using Lagrange multipliers, which represent the no-slip conditions along the fluid–structure interface. The implementation of this numerical technique is performed within the framework of the finite element method encoded in the SEPRAN software package (Segal, 2000). The essential feature of this approach is that independent discretizations of the computational domains are allowed. This means that the fluid finite element mesh is not altered or interrupted in any way by the presence of submerged structures. Conventional mesh update strategies, such as remeshing or arbitrary Lagrange–Euler techniques, consequently are superfluous.

The set of discretized linear algebraic equations is solved in a fully coupled manner. This leads to a solution procedure in which the fluid and structural unknowns are solved simultaneously, circumventing the judicious choice of the state variables to be transported

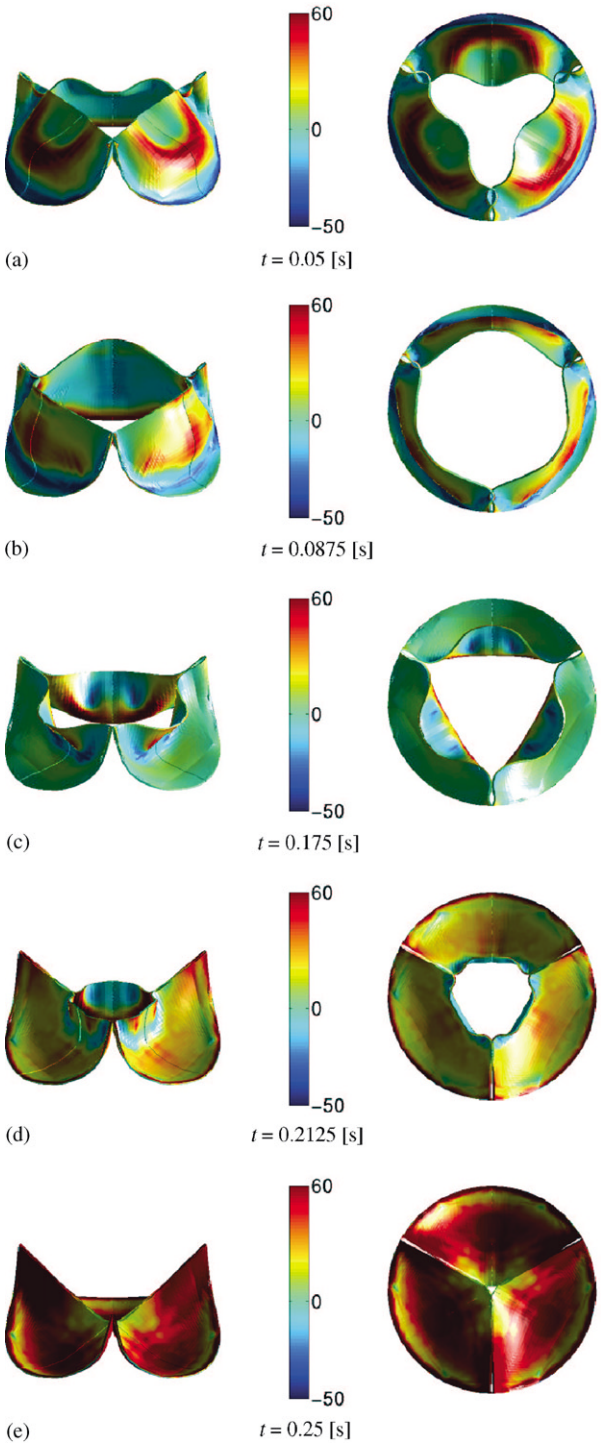

Fig. 8. Maximum principle Cauchy stresses in the leaflets during the systolic phase of the cardiac cycle. The stress scale is given in (kPa).

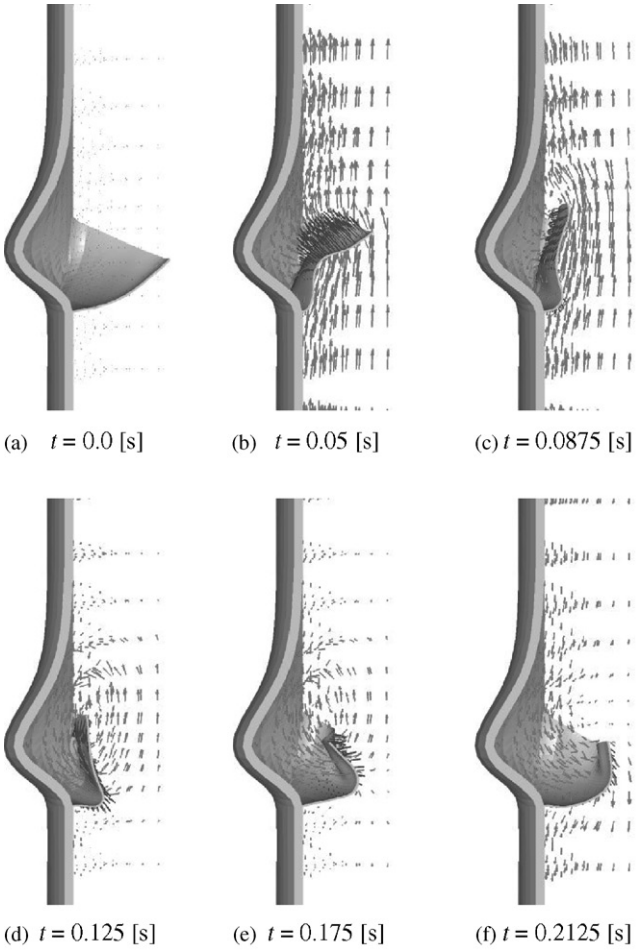

Fig. 9. Velocity vector field for six successive points in time.

from one system to the other, which is common practice in staggered procedures. However, the condition of the finite element matrix of the total system is affected, since the matrix entries display large variations caused by the difference in magnitude of the material parameters that describe the fluid and structure. Moreover, the solvability appears to be highly influenced by the number of additional Lagrange multipliers with respect to the number of fluid unknowns. For the application presented in this paper, the number of coupling constraints is chosen such that a BiCGStab iterative solver with a preconditioner based on an incomplete LU factorization using extra fill-in (Saad, 1996) is still feasible for reasonable amounts of both memory and CPU time. The convergence criterion for the BiCGStab iteration process is based on the maximum residual norm for which the tolerance is set to 10^{-4}. In the Newton–Raphson iteration process the convergence criterion is based on the norm of the change of the state variables in two successive iterations relative to the norm computed from the last converged solution with the tolerance set to 10^{-5}. These settings appeared to be sufficient for obtaining a solution indifferent to sharper tolerances.

The system is solved on a 64-bit Alpha 21264DP platform with a 667 MHz processor and an applicable memory allocation of 4 GB of which 20% is used. The ILU factorization takes 90% of the CPU time and, in practice, must be performed after two time steps on average, since the changing position of the structure in

the fluid domain involves a different mapping of the matrix entries associated with the Lagrange multipliers. For the valve model, having approximately 26,500 degrees of freedom, this resulted in a CPU time of 35 min per time step to obtain a converged solution. The application of a computationally more efficient solution strategy is currently under investigation.

The fictitious domain method is applied to simulate the response of a stented aortic valve to externally applied ventricular and aortic pressures. Results show that during systole the valve leaflets are moving with the fluid in an essentially kinematical process governed by the fluid motion. The model gives a detailed description of the flow phenomena in the valve. An accurate prediction of flow near the leaflets, however, remains complicated using the fictitious domain method, since the fictitious sources that represent the internal boundaries require an interpolation of the fluid velocity field to the fluid–leaflet interface.

The maximum pressure difference is taken such that the Reynolds and Strouhal number approximate 900 and 0.3, respectively. An analysis with the physiological Reynolds number ($Re = 4500$) combined with the physiological Strouhal number ($Sr = 0.06$) would lead to commonly expected numerical instabilities for a mesh coarseness as used in this model. Although a finer structural mesh did not significantly affect the solution, the application of a higher density for the fluid mesh requires further investigation. However, the valve kinematics, mechanics and hemodynamics are qualitatively in agreement with numerical and experimental studies previously done, see e.g. (Cacciola, 1998; Gao et al., 2000), (Black et al., 1991; Chandran et al., 1991; De Hart et al., 1998; Krucinski et al., 1993) and (Van Steenhoven and Veenstra, 1982), respectively. Moreover, we focus here on the three-dimensional application of the numerical method to study the importance of fluid–structure interaction rather than on the approximation of the physiological situation.

Contact between two adjacent leaflets has not been implemented in the applied computer code. Instead, it is expected that penetration of the leaflets is circumvented implicitly by using the fictitious domain method, since at the contact surface fluid velocities in the direction normal to this surface are suppressed. From Figs. 8(d) and (e) this is observed at the free edges of the leaflets. However, in Fig. 8(a) some penetration is seen, which is caused by the relative large displacement of the free edge within one time step. A decrease in time step size or an increase in the density $\mathscr{T}_{\gamma^i}$ near this area, i.e. adding more coupling constraints, would prevent penetration.

Although the model parameters are not such that a physiological correct behaviour is attained, the applied methods appear to be satisfactory in the three-dimensional computational analysis of fluid–structure interaction in the aortic valve. The development of valve models that more closely resemble the physiological situation in terms of anisotropic material behaviour, compliant aortic root and high Reynolds number flow, is currently under investigation.

References

Baaijens, F.P.T., 2001. A fictitious domain/mortar element method for fluid–structure interaction. International Journal for Numerical Methods in Fluids 35 (7), 743–761.

Black, M.M., Howard, I.C., Huang, X., Patterson, E.A., 1991. A three-dimensional analysis of a bioprosthetic heart valve. Journal of Biomechanics 24 (9), 793–801.

Brezzi, F., 1974. On the existence, uniqueness and approximation of saddle-point problems arising from Lagrange multipliers. RAIRO—Operations Research R2, 129–151.

Cacciola, G., 1998. Design, simulation and manufacturing of fiber reinforced polymer heart valves. Ph.D. Thesis, Eindhoven University of Technology, Eindhoven. http://www.mate.tue.nl.

Cacciola, G., Peters, G.W.M., Schreurs, P.J.G., 2000. A three-dimensional mechanical analysis of a stentless fibre-reinforced aortic valve prosthesis. Journal of Biomechanics 33 (5), 521–530.

Caro, C.G., Pedley, J.G., Schroter, R.C., Seed, W.A., 1978. The Mechanics of the Circulation. Oxford University Press, Oxford.

Chandran, K.B., Kim, H.H., Han, G., 1991. Stress distribution on the cusps of a polyurethane trileaflet heart valve prosthesis in the closed position. Journal of Biomechanics 24 (6), 385–395.

Cuvelier, C., Segal, A., Van Steenhoven, A.A., 1986. Finite Element Methods and Navier-Stokes Equations. D. Reidel, Dordrecht.

De Hart, J., 2002. Fluid–structure interaction in the aortic valve: a three-dimensional computational analysis. Ph.D. Thesis, Eindhoven University of Technology, Eindhoven. http://www.mate.tue.nl.

De Hart, J., Cacciola, G., Schreurs, P.J.G., Peters, G.W.M., 1998. A three-dimensional analysis of a fibre-reinforced aortic valve prosthesis. Journal of Biomechanics 31 (7), 629–638.

De Hart, J., Peters, G.W.M., Schreurs, P.J.G., Baaijens, F.P.T., 2000. A two-dimensional fluid–structure interaction model of the aortic valve. Journal of Biomechanics 33 (9), 1079–1088.

Donea, J., Giuliani, S., Halleux, J.P., 1982. An arbitrary Lagrangian–Eulerian finite element method for transient dynamic fluid–structure interactions. Computer Methods in Applied Mechanics and Engineering 33, 689–723.

Farhat, C., Lesoinne, M., LeTallec, P., 1998. Load and motion transfer algorithms for fluid/structure interaction problems with non-matching discrete interfaces: momentum and energy conservation, optimal discretization and application to aeroelastics. Computer Methods in Applied Mechanics and Engineering 157, 95–114.

Felippa, C.A., Park, K.C., Farhat, C., 1998. Partitioned analysis of coupled mechanical systems. Computer Methods in Applied Mechanics and Engineering 190, 3247–3270.

Gao, Z.B., Pandya, S., Hosein, N., Sacks, M.S., Hwang, N.H.C., 2000. Bioprosthetic heart valve leaflet motion monitored by dual camera stereo photogrammetry. Journal of Biomechanics 33 (2), 199–207.

Horsten, J.B.A.M., 1990. On the analysis of moving heart valves: a numerical fluid–structure interaction model. Ph.D. Thesis, Eindhoven University of Technology, Eindhoven.

Krucinski, S., Vesely, I., Dokainish, M.A., Campbell, G., 1993. Numerical simulation of leaflet flexure in bioprosthetic valves mounted on rigid and expansile stents. Journal of Biomechanics 26 (8), 929–943.

Lesoinne, M., Farhat, C., 1998. Improved staggered algorithms for the serial and parallel solution of three-dimensional nonlinear transient aeroelastic problems. In: Oñate, E.O., Idelsohn, S. (Eds.),

Proceedings of the WCCM IV Conference on Computational Mechanics. CIMNE, Barcelona.

Makhijani, V.B., Yang, H.Q., Dionne, P.J., Thubrikar, M.J., 1997. Three-dimensional coupled fluid–structure simulation of pericardial bioprosthetic aortic valve functioning. ASAIO Journal 43 (5), M387–M392.

Peskin, C.S., McQueen, D.M., 1995. A general method for the computer simulation of biological systems interacting with fluids. Symposia of The Society for Experimental Biology 49, 265–276.

Rutten, M.C.M., 1998. Fluid-solid interaction in large arteries. Ph.D. Thesis, Eindhoven University of Technology, Eindhoven. http://www.mate.tue.nl.

Saad, Y., 1996. Iterative Methods for Sparse Linear Systems. PWS Publishing Company, Boston.

Segal, G., 2000. SEPRAN Introduction, User's Manual, Programmer's Guide and Standard Problems. Ingenieursbureau SEPRA, Leidschendam.

Van Steenhoven, A.A., Veenstra, P.C., 1982. The effect of some hemodynamic factors on the behaviour of the aortic valve. Journal of Biomechanics 15 (12), 941–950.

Wall, W.A., Ekkehard, R., 1998. Fluid–structure interaction based upon a stabilized (ALE) finite element method. In: Oñate, E.O., Idelsohn, S. (Eds.), Proceedings of the WCCM IV Conference on Computational Mechanics. CIMNE, Barcelona.